Rate dependent behaviors of nickel-based microcapsules

Xin Zhang, Pengfei Wang, Dawei Sun, Xin Li, T. X. Yu, En-Hua Yang, and Jinglei Yang

Articles you may be interested in

Rate dependent behaviors of nickel-based microcapsules

Xin Zhang,[1,2] Pengfei Wang,[3] Dawei Sun,[4,5] Xin Li,[6] T. X. Yu,[4] En-Hua Yang,[2,a)] and Jinglei Yang[4,a)]

[1]Interdisciplinary Graduate School, Nanyang Technological University, 50 Nanyang Avenue, Singapore 639798
[2]School of Civil and Environmental Engineering, Nanyang Technological University, 50 Nanyang Avenue, Singapore 639798
[3]CAS Key Laboratory of Mechanical Behavior and Design of Materials, Department of Modern Mechanics, University of Science and Technology of China, Hefei 230026, China
[4]Department of Mechanical and Aerospace Engineering, The Hong Kong University of Science and Technology, Clear Water Bay, Kowloon, Hong Kong, China
[5]College of Materials Science and Engineering, Beijing University of Technology, Beijing 100124, China
[6]Institute of Applied Mechanics and Biomedical Engineering, Taiyuan University of Technology, Taiyuan 030024, China

In this work, nickel-based microcapsules with liquid core were fabricated through an electroless plating approach. The quasi-static and high speed impact behaviors of microcapsules were examined by in-house assembled setups which are able to evaluate properties of materials and structures in microlevel accurately. Results indicated that the fabricated microcapsules showed strong rate sensitivity and the nominal strength of the capsule increased (up to 62.1%) with the increase in loading rates (up to 8200 s^{-1}). The reduced modulus of nickel-based microcapsules was three orders of magnitude larger than that of the traditional microcapsules. The findings revealed that the fabricated nickel-based microcapsules produced remarkable performances for both static and dynamic loading applications. A high speed camera with stereo microscope was used to observe the failure mode of the microcapsule during the impact, which is of great importance to study the mechanical behaviours of materials and structures. Different failure modes were identified as multi-cracks with more rough and tortuous fracture surfaces and debris were observed for the samples subject to impact loading. Finite element method was employed to further understand the physical phenomenon which fitted well with the experimental results. These results could inspire more fundamental studies on the core-shell microstructures and potential applications in multifunctional materials. *Published by AIP Publishing.* https://doi.org/10.1063/1.5025363

During the past few decades, microcapsules with liquid core and solid shell structure have been widely used to engage self-healing functionality into composites such as self-healing fibre-reinforced polymer composite and self-healing concrete.[1,2] Self-healing enables repair of damage in materials partially or even completely without external intervention.[3] To fabricate healant-loaded and functional microcapsules, different approaches and different materials have been investigated.[4–9] However, in most cases, the introduction of microcapsules may decrease the mechanical properties of the composites because the strength of individual microcapsules was weak. It is of great importance to investigate the mechanical properties of individual microcapsules.

Most researchers studied the quasi-static compressive behavior of microcapsules.[10,11] The peak load of microcapsules under quasi-static compression varied from 1 μN to 60 mN with the diameters varied from 40 μm to 400 μm.[12–15] The strength of individual microcapsules was quite weak due to the use of organic polymer or silica as capsule shell which would reduce the mechanical properties of composite. The inorganic microcapsules developed in this study were much stronger than other traditional microcapsules. However, they are able to

rupture even in an epoxy matrix under certain loading conditions, which trigger the self-healing process of the composite.

Dong et al.[16] investigated the dynamic response of big thin-walled hollow spheres. Their results suggested that deformation and buckling mode of spheres were sensitive to the loading rate. Zhang et al.[17] studied the dynamic behaviors of viscoelastic thin-walled hollow spheres. It was found that the input kinetic energy was approximately 2.5–3 times the deformation energy in quasi-static compression. The dynamic responses of big solid spherical particles were studied by many other researchers,[18–20] and more failure modes in the low velocity loading were found when compared with the high velocity impact.

However, the dynamic properties and simulations of microcapsules have rarely been investigated. Garza-Cruz and Nakagawa[21] employed finite element method (FEM) to investigate the development of stresses on a hollow glass microsphere during its uniaxial compression, implying that larger stresses were concentrated near the contact region. Wang et al.[22] and Li et al.[23] conducted the high speed compression on single microcapsules. The maximum velocities of their high speed compressions were 0.2 mm/s and 4.9 mm/s, which were both far from enough to investigate the dynamic response of individual microcapsule. As a result, the investigation on the quasi-static and dynamic response of microcapsules is in great need.

a)Authors to whom correspondence should be addressed: maeyang@ust.hk and ehyang@ntu.edu.sg

Nickel-based microcapsules with liquid core were fabricated through an electroless plating approach [Fig. 1(a)]. First, palladium particles were absorbed on the surface of emulsified liquid wax monodisperse droplets as catalyst [Fig. 1(a)]. Second, the metal shell was generated through the chemical plating. The detailed fabrication method can be found in the supplementary material. This approach provides the possibility of directly forming a robust metal layer around liquid droplets, which inspires potential encapsulation of the multifunctional material. In addition, the approach is multipurpose which can also encapsulate other hydrophobic liquids like phase change materials, epoxy resins, and liquid wax to apply for phase change, self-healing, and antifriction purposes. The fabricated microcapsules had a diameter of approximately 270 μm [Fig. 1(b)] and a constant shell thickness of about 6.7 μm [Fig. 1(c)], which were measured by a field emission scanning electron microscope (FESEM, Jeol, JSM-7600F). The diameter of each microcapsule was measured using an optical microscope (Olympus, SZX7). The microcapsules with diameter from 245 μm to 295 μm were filtered for test. Computerized tomography (CT) scans (Fein Focus, Y.Fox) were used to evaluate whether the core material was filled full. As shown in Fig. 1(d), the bright circle indicates the metal shell while the well distributed off-white color inside the circle indicates the core material. The observation deduced that the core material of the fabricated microcapsule fill in the metal shell to the full.[24]

As a result, a low speed loading setup [Figs. 2(a) and 2(b)] and a micro impact setup [Figs. 2(c) and 2(d)] were developed and modified by authors. The detailed description of these setups can be found in the supplementary material. Three constant test speeds at 1 μm/s, 10 μm/s, and 100 μm/s were adopted by using the low speed loading setup. Two micro impact apparatuses were established, which were direct micro impact apparatus and Taylor micro impact apparatus.[25,26] In direct impact apparatus, the impactor was freely drop to hit the capsule, while the microcapsule was dropped together with the impactor in Taylor impact apparatus. Two impact velocities at 0.3 m/s and 2.2 m/s were conducted. The loading speeds were obtained from images captured by the high speed camera. The developed micro impact setup can be used to investigate the dynamic strength, buckling deformation, and fracture mode of micro structure (e.g., microcapsule) at dynamic loading. More than 10 samples were tested
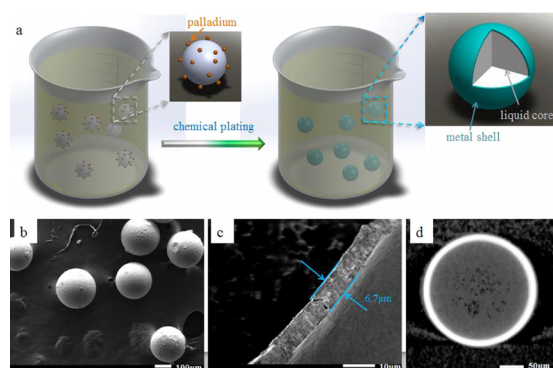

FIG. 1. (a) Schematic of the fabrication of nickel-based microcapsules with liquid core, SEM images for (b) well-dispersed microcapsules and (c) shell profile, and (d) CT scanned image of a single microcapsule.
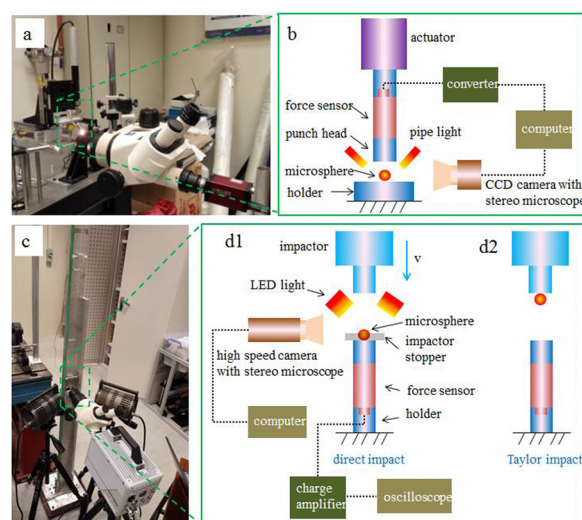

FIG. 2. (a) and (b) schematic of low speed loading setup and (c) and (d) micro impact setup.

for each loading condition. An impactor stopper was used in the direct impact apparatus to ensure samples achieving the same deformation of approximately 100 μm. The developed apparatuses are able to accurately evaluate the properties of materials and structures at the microlevel. The calculation of nominal strength, integrated failure strain, and loading rates can be found in the supplementary material. From the images captured by a high speed camera, it is found that the velocity of impactor in the micro impact apparatus remained constant during the compression. Therefore, it is reasonable to assume that the microcapsules were subjected to constant loading rates both at the low and the high speed impacts.[27]

As shown in Fig. 3(a), the nominal strength of microcapsules increase significantly (up to 62.1%) with the increase in the loading rate (up to 8200 s^{-1}). The increase is more pronounced at higher loading rates beyond 10^2 s^{-1}, in particular. This indicates that significant loading rate effects exist when the microcapsules are subjected to impact, which can be attributed to three aspects. First, the core shell structure provides the rate effect during the impact due to the inertia effect and higher order fracture mode.[28] Second, the nickel material may provide the strain rate effect during the impact.[29] Last but not least, the filled liquid in the structure may generate higher hydrostatic pressure during impact which may dissipate more energy compared to low rate loading. All these factors contribute to the significant loading rate effect of the microcapsule. The fabricated nickel-based microcapsule is robust with a nominal strength of more than 20 MPa at high loading rates. That is because the high strength of nickel material and the high loading rate effect of the structure can enhance the strength of the integral microcapsule significantly.

These findings suggested that the fabricated microcapsule performed well in both static and dynamic loadings. The average nominal strength determined from the direct impact test is similar to that from Taylor impact test at a high loading rate. This observation implies that the contact force between the impactor and the microcapsule and the contact force between the microcapsule and the holder can be regarded as the same value. It provides evidence that the
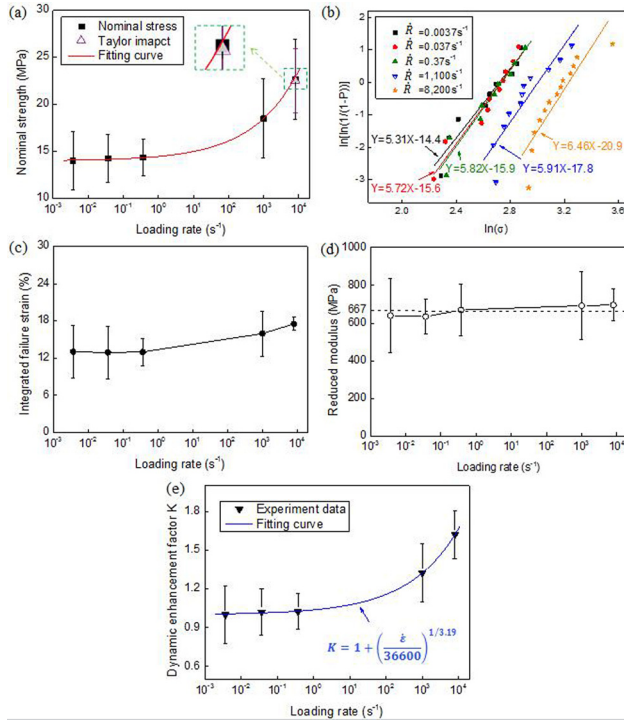
FIG. 3. (a) Nominal strength, (b) Weibull distribution of strength, (c) integrated failure strain, (d) reduced modulus, and (e) dynamic enhancement factor of microcapsules at different loading rates.

stress wave propagation in the microcapsule reached equilibrium state during the high velocity impact test.[30]

The scattering property of the strength of an individual microcapsule is investigated by using the Weibull distribution method.[31] The Weibull distribution model can be expressed by the following equation:

$$P(\sigma) = 1 - \exp\left[-\left(\frac{\sigma}{\sigma_0}\right)^m\right], \quad (1)$$

where m is the Weibull shape factor, which indicates the scattering in the strength of individual microspheres. σ_0 represents the scale parameter.

Applying double logarithm of Eq. (1), a linear relationship can be drawn between $\ln\left[\ln\left(1/(1 - P(\sigma))\right)\right]$ and $\ln\sigma$ with slope value of m, as shown in the following equation:

$$\ln\left[\ln\left(\frac{1}{1 - P(\sigma)}\right)\right] = m\ln\sigma - m\ln\sigma_0. \quad (2)$$

The higher value of m indicates a more uniform strength and vice versa.[32] The value of m can be obtained by fitting the data as shown in Fig. 3(b). The Weibull shape factors are 5.31, 5.72, 5.82, 5.91, and 6.46 for microcapsules at loading rates of 0.0037 s^{-1}, 0.037 s^{-1}, 0.37 s^{-1}, 1100 s^{-1}, and 8200 s^{-1}, respectively. The gradually increased Weibull shape factor with the increased loading rate implies that the microcapsule tends to perform more uniformly during a high speed impact, which may be attributed to that the flaws (e.g., cracks) in the microcapsule during the fabrication can generate more negative effects during the quasi-static compression, which leads to a larger scatter during the test while the flaws may not cause severe fracture during impact loading. Meanwhile, all the

Weibull shape factors of the nickel microcapsules are larger than 5.3, which indicate a narrow strength distribution and a good fabrication process. After the comparison with the works from others, it is found that the Weibull shape factor of the fabricated nickel shell microcapsule is higher than the dynamic compression of fiber reinforced concrete (m values from 1.0 to 1.2),[33] and higher than the compression of a silica sand (m values at 3.3)[34] and close to or higher than the tension of carbon nanotube (CNT) fiber and commercial carbon fiber (m values from 5.65 to 6.13).[27] The findings confirm that both the reproducibility of the testing results and the fabrication process are acceptable.

The integrated failure strain also increases with loading rates but of less pronounced. It remains steady at a low loading rate while increases slightly at high loading rates [Fig. 3(c)]. This may be attributed to that only single crack was formed and propagated through the lowest energy dissipation path in the quasi-static compression while multiple cracks can be generated during dynamic compression which dissipates more energy and further improved the toughness.[35] Another plausible mechanism could be due to the presence of liquid core inside the microcapsule which provides strong hydrostatic pressure to support the shell during the dynamic compression and increased the failure strain of the microcapsule.

The influences of loading rates on the modulus of microcapsule were studied. The modulus can be calculated from Hertz theory,[36,37] which determines the contact force of sphere compressed between two flat rigid surfaces, as shown in the following equation:

$$F = \frac{4R^{1/2}}{3}\frac{E}{1 - \nu^2}\left(\frac{d}{2}\right)^{3/2}, \quad (3)$$

where F is the contact force, R, E, ν, and d are the radius, the modulus, the Poisson's ratio, and the deflection of the microcapsule, respectively. $E_r = E/(1 - \nu^2)$ is defined as the reduced modulus of the microcapsule.

As seen in Fig. 3(d), the reduced moduli of microcapsules increase slightly with the increase in loading rates due to limited strain hardening effects of the metal shell. The reduced modulus of the nickel-based microcapsule is high with a mean value of 667 MPa, which is about three orders of magnitude higher than that of the alginate microcapsule.[22] The value of ν can be taken as 0.5 since the microcapsules are assumed to be uncompressible.[38] As a result, the modulus of nickel-based microcapsule is around 500 MPa.

To evaluate the rate dependence of the fabricated nickel-based microcapsules, the dynamic enhancement factor K is introduced, which can be expressed in Eq. (4) that deduced from Cowper-Symonds model (C-S model)[39,40]

$$K = 1 + \left(\frac{\dot{\varepsilon}}{D}\right)^{1/q}, \quad (4)$$

where $\dot{\varepsilon}$ is the loading rate, and D and q are constants for specific material in C-S model. The compressive strength at a loading speed of 1 μm/s was used as the reference strength. K can be calculated by the strength under corresponding loading rate divided by the reference strength.

Figure 3(e) shows the dynamic enhancement factor of microcapsules at different loading rates. The experimental

results fit well with the C-S model ($R^2 > 0.999$) and K can be expressed as

$$K_{Nickel} = 1 + \left(\frac{\dot{\varepsilon}}{36\,600}\right)^{1/3.19}. \tag{5}$$

As can be seen, the effect is more pronounced at high loading rates.

To further understand the physical phenomenon of the compression of individual microcapsule, ABAQUS/EXPLICIT is employed. The model consisted of two rigid plates, one spherical shell, and one spherical core [Fig. 4(a)]. Quadrilateral shell mesh and hexahedral solid mesh are used for the shell and core materials, respectively, as shown in Figs. 4(b) and 4(c).

A Nano-indenter (Agilent G200) is used to evaluate the elastic modulus of fabricated nickel material.[41,42] The obtained Young's modulus is 98.1 ± 7.1 GPa. Some other basic mechanical properties of nickel material can be obtained from the literature reviews.[29,43] The Johnson-Cook hardening factor is 0.025, while the fracture strain is 2%. The dynamic viscosity of liquid wax was tested by a rheometer (TA DHR-2), which shows a relatively constant viscosity of 0.026 Pa s no matter the shear rate. The us-up model in equation of state is employed to simulate the liquid material which can be introduced to solve the fluid-structure interaction by using explicit simulation method. The compression velocities varied from 10^{-4} to 25 m/s.

The typical load deflection curves of an individual nickel-based microcapsule under impact at a loading rate around 10^4 s^{-1} and 10^5 s^{-1} are depicted in Fig. 4(d). The result reveals that the contact force between the impactor and the sphere and the contact force between the sphere and the holder fit well with each other at a loading rate around 10^4 s^{-1}, indicating that a stress equilibrium state is achieved during the impact. This phenomenon fits well with the experimental results from direct impact and Taylor impact. In other words, it is accurate enough to measure the impact force during the experiment by using the dynamic impact setup for microcapsules developed in our laboratory. However, the equilibrium state is not achieved when the loading rate increases to 10^5 s^{-1} because of

the short time for stress wave propagation to reach equilibrium in the specimen. The nominal stress is also investigated through FEM. As shown in Fig. 4(e), the nominal stress from the simulation fits well with experimental measurement. A similar trend is also observed which indicates the reliability of the conducted mechanical model for individual microcapsule. It can also predict the strength of microcapsule at a desired loading rate which may not be very convenient and easy to detect during an experiment.

The analysis of the fracture mode is essential to further investigate the dynamic response of microcapsules. Consequently, the fracture mode of the microcapsule was recorded by a digital camera and a high speed camera with a stereo microscope. As shown in Fig. 5(a), a single crack propagated through (from the top to the bottom) the shell of microcapsule during the quasi-static compression. Figure 5(b) shows the typical failure mode of microcapsule subject to impact loading. The response of microcapsule under impact was captured by the high speed camera with a 20 μs time interval. As demonstrated in Figs. 5(b3) and 5(b4), one dominant crack appeared at the backside of the capsule while the liquid ejected from the right side of the microcapsule which implied that at least two cracks were formed during the impact. The localized failure of the microcapsule suggested that multi-crack may form under impact loading. The observations provided deformation and failure mechanism of microstructures, which are significant to study mechanical behaviours of structures. The FESEM images confirmed that a single crack with a clean fracture surface was the dominant failure mode in the nickel-based microcapsule under quasi-static loading [Figs. 5(a5) and 5(a6)] and multi-cracks with rough zigzag fracture surface and debris were observed in the capsule subject to the high speed impact [Figs. 5(b5) and 5(b6)]. All of the observation supported that multiple cracks can be generated during the dynamic compression which dissipated more energy and further improved the toughness of the microcapsule.[35]

The fracture processes under loading rate of 0.37 s^{-1} compression (quasi-static), 8200 s^{-1} impact (dynamic), and
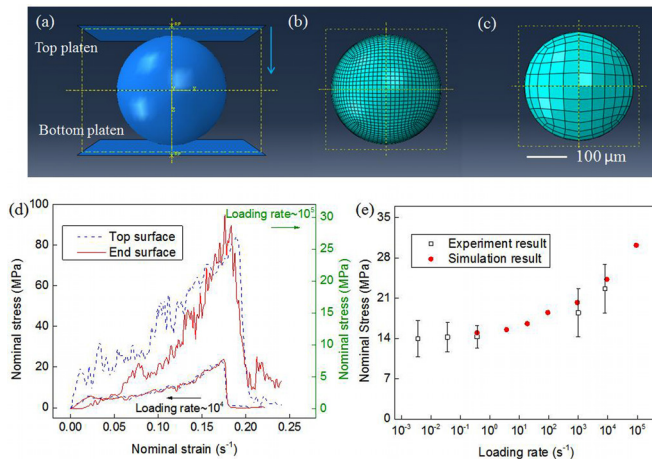

FIG. 4. (a) Modeling of compression of individual microcapsule, (b) quadrilateral mesh for shell, and (c) hexahedral mesh for liquid core. (d) Typical load versus deflection curve of the compression at loading rate around 10^4 and 10^5 s^{-1} through FEM; (e) nominal stress versus loading rate through experiment and simulation.
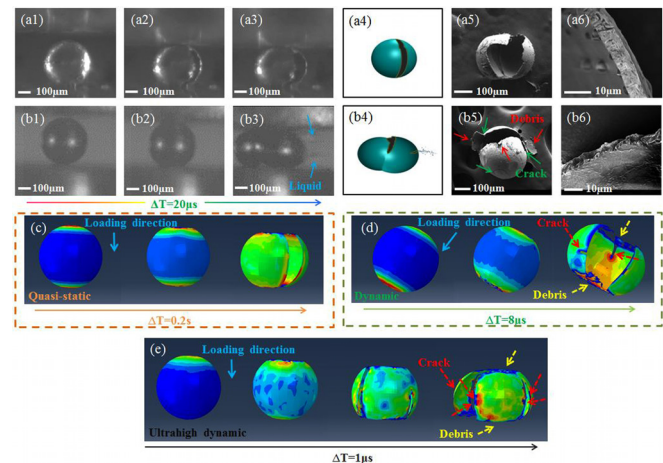

FIG. 5. Progressive failure process of individual microcapsule under compression: (a1)–(a3) at low loading rate and schematic image (a4) with SEM image of the compressed microcapsule (a5) and fractured shell (a6); (b1)–(b3) at high loading rate and schematic image (b4) with SEM image of the impacted microcapsule (b5) and fractured shell (b6); at quasi-static loading (c), at dynamic loading (d), and at ultrahigh dynamic loading (e) with time intervals of 0.2 s, 8 μs, and 1 μs, respectively, by using FEM.

82 000 s^{-1} impact (ultrahigh dynamic) through simulation were also studied and shown in Figs. 5(c), 5(d), and 5(e) with a time interval of 0.2 s, 8 μs, and 1 μs, respectively. The stress concentrated at both top and end surfaces of the microcapsule and achieved equilibrium state quickly at both quasi-static and dynamic loading conditions. However, during ultrahigh dynamic condition, an obvious non-equilibrium state was observed at the early stage of impact as the stress concentrated only at the top surface of the microcapsule. The fracture morphology through the simulation was quite similar with that of individual microcapsule (FESEM image) after experiment since single overall crack [Fig. 5(c)] of microcapsule from quasi-static loading and many cracks and debris [Fig. 5(d)] from dynamic loading were observed. Moreover, more cracks were observed at ultrahigh dynamic loading [Fig. 5(e)], which confirmed our conclusion in the experiment part.

In summary, nickel-based microcapsules were fabricated through an electroless plating approach. Low speed loading and microimpact apparatuses were built up. This study provides a good approach to systematically investigate the mechanical behavior of individual microcapsule at different loading rates. Results indicated that the fabricated microcapsules showed strong rate sensitivity and the nominal strength increased (up to 62.1%) with the increased loading rates, which enabled it suitable for dynamic applications. The reduced modulus of nickel-based microcapsules was three orders of magnitude larger than traditional microcapsules. A high speed camera was used to observe the failure mode of the specimen during the impact. Different failure modes were identified as multi-cracks with more rough and tortuous fracture surfaces and debris were observed for the specimens subject to impact loading. FEM was employed to further understand the physical mechanism of the compression and impact of individual microcapsule, which also proved the reliability of the experiment.

See supplementary material for the detailed synthesis approach for nickel-based microcapsules, the fabrication of low speed loading and microimpact setups, and parameters calculation for fabricated microcapsules.

[1]J. Y. Wang, K. Van Tittelboom, N. De Belie, and W. Verstraete, Constr. Build. Mater. **26**(1), 532 (2012).

[2]S. Zwaag, *Self Healing Materials: An Alternative Approach to 20 Centuries of Materials Science* (Springer Science+ Business Media BV, 2008).

[3]R. C. R. Gergely, W. A. S. Cruz, B. P. Krull, E. L. Pruitt, J. Wang, N. R. Sottos, and S. R. White, Adv. Funct. Mater. **28**(2), 1704197 (2018).

[4]T. Bollhorst, K. Rezwan, and M. Maas, Chem. Soc. Rev. **46**(8), 2091 (2017).

[5]S. A. Odom, T. P. Tyler, M. M. Caruso, J. A. Ritchey, M. V. Schulmerich, S. J. Robinson, R. Bhargava, N. R. Sottos, S. R. White, M. C. Hersam, and J. S. Moore, Appl. Phys. Lett. **101**(4), 043106 (2012).

[6]F. Peng, N. N. Deng, Y. F. Tu, J. C. M. van Hest, and D. A. Wilson, Nanoscale **9**(15), 4875 (2017).

[7]M. D. Hager, P. Greil, C. Leyens, S. van der Zwaag, and U. S. Schubert, Adv. Mater. **22**(47), 5424 (2010).

[8]T. Si, C. S. Yin, P. Gao, G. B. Li, H. Ding, X. M. He, B. Xie, and R. X. Xu, Appl. Phys. Lett. **108**(2), 021601 (2016).

[9]Q. Wu, C. Y. Yang, J. X. Yang, F. S. Huang, G. L. Liu, Z. Q. Zhu, T. Si, and R. X. Xu, Appl. Phys. Lett. **112**(7), 071601 (2018).

[10]D. F. do Nascimento, J. A. Avendano, A. Mehl, M. J. B. Moura, M. S. Carvalho, and W. J. Duncanson, Sci. Rep.-Uk **7**, 11898 (2017).

[11]A. Ghaemi, A. Philipp, A. Bauer, K. Last, A. Fery, and S. Gekle, Chem. Eng. Sci. **142**, 236 (2016).

[12]H. Zhang, P. F. Wang, and J. L. Yang, Compos. Sci. Technol. **94**, 23 (2014).

[13]W. P. Ma, W. Zhang, Y. Zhao, and S. J. Wang, J. Appl. Polym. Sci. **133**(19), 43720 (2016).

[14]K. Kim, J. Cheng, Q. Liu, X. Y. Wu, and Y. Sun, J. Biomed. Mater. Res. Part A **92**(1), 103 (2010).

[15]L. Y. Lv, E. Schlangen, Z. X. Yang, and F. Xing, Materials **9**(12), 1025 (2016).

[16]X. L. Dong, Z. Y. Gao, and T. Yu, Int. J. Impact Eng. **35**(8), 717 (2008).

[17]X. W. Zhang, Z. Tao, and Q. M. Zhang, Lat. Am. J. Solids Struct. **11**(14), 2607 (2014).

[18]A. D. Salman, G. K. Reynolds, J. S. Fu, Y. S. Cheong, C. A. Biggs, M. J. Adams, D. A. Gorham, J. Lukenics, and M. J. Hounslow, Powder Technol. **143–144**, 19 (2004).

[19]R. G. Rinaldi, L. Manin, C. Bonnard, A. Drillon, H. Lourenco, and N. Havard, Procedia Eng. **147**, 348 (2016).

[20]O. Cermik, H. Ghaednia, and D. B. Marghitu, in *Acoustics and Vibration of Mechanical Structures—AVMS-2017* (Springer, 2018), p. 33.

[21]T. V. Garza-Cruz and M. Nakagawa, Granular Matter **14**(3), 309 (2012).

[22]C. Wang, C. Cowen, Z. Zhang, and C. R. Thomas, Chem. Eng. Sci. **60**(23), 6649 (2005).

[23]Z. Li, Z. Zhang, and C. Thomas, Innovative Food Sci. Emerging Technol. **34**, 44 (2016).

[24]X. Zhang, P. F. Wang, H. S. Neo, G. H. Lim, A. A. Malcolm, E. H. Yang, and J. L. Yang, Mater. Des. **92**, 621 (2016).

[25]I. Elnasri, S. Pattofatto, H. Zhao, H. Tsitsiris, F. Hild, and Y. Girard, J. Mech. Phys. Solids **55**(12), 2652 (2007).

[26]P. F. Wang, S. L. Xu, Z. B. Li, J. L. Yang, C. Zhang, H. Zheng, and S. S. Hu, Mater. Sci. Eng. A **620**, 253 (2015).

[27]P. Wang, X. Zhang, R. V. Hansen, G. Sun, H. Zhang, L. Zheng, T. X. Yu, G. Lu, and J. Yang, Carbon **102**, 18 (2016).

[28]P. Li, N. Petrinic, C. R. Siviour, R. Froud, and J. M. Reed, Mater. Sci. Eng. A **515**(1-2), 19 (2009).

[29]R. Schwaiger, B. Moser, M. Dao, N. Chollacoop, and S. Suresh, Acta Mater. **51**(17), 5159 (2003).

[30]X. Zhang, B. Hou, and Y. L. Li, Explos. Shock Waves **31**(3), 256 (2011).

[31]F. W. Zok, J. Am. Ceram. Soc. **100**(4), 1265 (2017).

[32]G. Z. Sun, J. H. L. Pang, J. Y. Zhou, Y. N. Zhang, Z. Y. Zhan, and L. X. Zheng, Appl. Phys. Lett. **101**(13), 131905 (2012).

[33]Z. L. Wang, Y. S. Liu, and R. F. Shen, Constr. Build. Mater. **22**(5), 811 (2008).

[34]G. R. McDowell and J. P. De Bono, Geotechnique **63**(11), 895 (2013).

[35]S. S. Wang, M. H. Zhang, and S. T. Quek, Constr. Build. Mater. **31**, 1 (2012).

[36]M. Rubsam, A. F. Mertz, A. Kubo, S. Marg, C. Jungst, G. Goranci-Buzhala, A. C. Schauss, V. Horsley, E. R. Dufresne, M. Moser, W. Ziegler, M. Amagai, S. A. Wickstrom, and C. M. Niessen, Nat. Commun. **8**, 1250 (2017).

[37]L. Pastewka and M. O. Robbins, Appl. Phys. Lett. **108**(22), 221601 (2016).

[38]E. S. Chan, T. K. Lim, W. P. Voo, R. Pogaku, B. T. Tey, and Z. B. Zhang, Particuology **9**(3), 228 (2011).

[39]X. Chen, Y. L. Li, Z. Zhi, Y. Z. Guo, and N. Ouyang, Carbon **61**, 97 (2013).

[40]D. M. Wang and Z. Y. Bai, Mater. Des. **77**, 59 (2015).

[41]J. Zeisig, J. Hufenbach, H. Wendrock, T. Gemming, J. Eckert, and U. Kuhn, Appl. Phys. Lett. **108**(14), 143103 (2016).

[42]G. Singh, R. L. Narayan, A. M. Asiri, and U. Ramamurty, Appl. Phys. Lett. **108**(18), 181903 (2016).

[43]W. C. Xu and P. Q. Dai, Rare Met. Mater. Eng. **38**(12), 2075 (2009).